Astronomy & Astrophysics manuscript no. chplus˙detection˙paper
January 19, 2013

Letter to the Editor

Detection of CH^+ emission from the disc around HD 100546⋆

W.-F. Thi[1], F. Ménard[1], G. Meeus[2], C. Martin-Zaïdi[1], P. Woitke[3,4,5,1], E. Tatulli[1], M. Benisty[6], I. Kamp[7], I. Pascucci[8], C. Pinte[1], C. A. Grady[9], S. Brittain[10], G. J. White[11,12] C. D. Howard[13], G. Sandell[13], C. Eiroa[2]

[1] UJF-Grenoble 1 / CNRS-INSU, Institut de Planétologie et d'Astrophysique (IPAG) UMR 5274, Grenoble, F-38041, France
e-mail: Wing-Fai.Thi@obs.ujf-grenoble.fr
[2] Dep. de Física Teórica, Fac. de Ciencias, UAM Campus Cantoblanco, 28049 Madrid, Spain
[3] University of Vienna, Dept. of Astronomy, Türkenschanzstr. 17, A-1180 Vienna, Austria
[4] School of Physics & Astronomy, University of St. Andrews, North Haugh, St. Andrews KY16 9SS, UK
[5] UK Astronomy Technology Centre, Royal Observatory, Edinburgh, Blackford Hill, Edinburgh EH9 3HJ, UK
[6] Max Planck Institute for Astronomy, Königstuhl 17 D-69117, Heidelberg, Germnay
[7] Kapteyn Astronomical Institute, P.O. Box 800, 9700 AV Groningen, The Netherlands
[8] Space Telescope Science Institute, 3700 San Martin Drive, Baltimore, MD 21218, USA
[9] Eureka Scientific and Exoplanets and Stellar Astrophysics Lab, NASA Goddard Space Flight Center, Code 667, Greenbelt, MD, 20771, USA
[10] Clemson University, Clemson, SC, USA
[11] Department of Physics & Astronomy, The Open University, Milton Keynes MK7 6AA, UK
[12] The Rutherford Appleton Laboratory, Chilton, Didcot, OX11 OQL, UK
[13] SOFIA-USRA, NASA Ames Research Center, Mailstop 211-3 Moffett Field CA 94035 USA

Received 2011; accepted 2011

ABSTRACT

Despite its importance in the thermal balance of the gas and in the determination of primeval planetary atmospheres, the chemistry in protoplanetary discs remains poorly constrained with only a handful of detected species. We observed the emission from the disc around the Herbig Be star HD 100546 with the PACS instrument in the spectroscopic mode on board the Herschel Space Telescope as part of the GaS in Protoplanetary Systems (GASPS) programme and used archival data from the DIGIT programme to search for the rotational emission of CH^+. We detected in both datasets an emission line centred at 72.16 μm that most likely corresponds to the J=5-4 rotational emission of CH^+. The J=3-2 and 6-5 transitions are also detected albeit with lower confidence. Other CH^+ rotational lines in the PACS observations are blended with water lines. A rotational diagram analysis shows that the CH^+ gas is warm at 323^{+2320}_{-151} K with a mass of $\sim 3 \times 10^{-14}$-5×10^{-12} $M_\odot$. We modelled the CH^+ chemistry with the chemo-physical code ProDiMo using a disc density structure and grain parameters that match continuum observations and near- and mid-infrared interferometric data. The model suggests that CH^+ is most abundant at the location of the disc rim at 10-13 AU from the star where the gas is warm, which is consistent with previous observations of hot CO gas emission.

Key words. Circumstellar discs, Astrochemistry

1. Introduction

Planets are formed in discs around young stars. The building of planets is intimately linked to the grain-growth process and the disc's chemical evolution (Bergin et al. 2007). The chemical and temperature profiles of discs determine the chemical composition of the gas that will eventually be incorporated into a planet's atmosphere, once a solid ∼ 10 Earth mass core is formed (Armitage 2010). Millimetre observations of molecules in discs probe the outer cold part (Dutrey et al. 1997; van Zadelhoff et al. 2001; Thi et al. 2004; Semenov et al. 2005; Henning et al. 2010; Öberg et al. 2010, e.g.). Minor species located in the inner disc, such as C_2H_2 and HCN, were observed with the Spitzer Space Telescope (Carr & Najita 2008; Pascucci & Sterzik 2009; Lahuis et al. 2006; Pontoppidan et al. 2010). Gas-phase carbon is believed to be locked into C^+, C, and CO. However, a significant fraction of the carbon can be locked into CH and CH^+, which are observed in the optical in diffuse clouds.

The Herschel Space Telescope permits observations of hydrides and their ions (OH, OH^+, CH, CH^+, ...), and warm light molecular gas (e.g., H_2O), which all emit in the far-infrared. Rotational lines of CH^+ at 300-500 K in the far-IR have been observed by ISO towards the NGC7027 PDR (Cernicharo et al. 1997). The isotopologue $^{13}CH^+$ J=1-0 was detected in absorption in the diffuse medium by Falgarone et al. (2005). The lowest rotational transition was detected in emission in the Orion Bar (Naylor et al. 2010; Habart et al. 2010) and in absorption towards DR 21 (Falgarone et al. 2010) with Herschel. The neutral counterpart CH has also been detected in the diffuse medium by Herschel (Qin et al. 2010; Gerin et al. 2010). In this letter, we discuss the detection of emission lines with Herschel that we assign to the rotational transition of CH^+ from the disc around the 10 Myrs old Herbig Be star HD 100546 (M_*= 2.2 $M_\odot$, L_*= 27 $L_\odot$, $T_{\rm eff}$= 10500 K) located at 103 pc (van den Ancker et al. 1997). HD 100546 shows a very rich gas and a solid spectrum in the infrared and millimetre

⋆ Herschel is an ESA space observatory with science instruments provided by Principal Investigator consortia. It is open for proposals for observing time from the worldwide astronomical community.

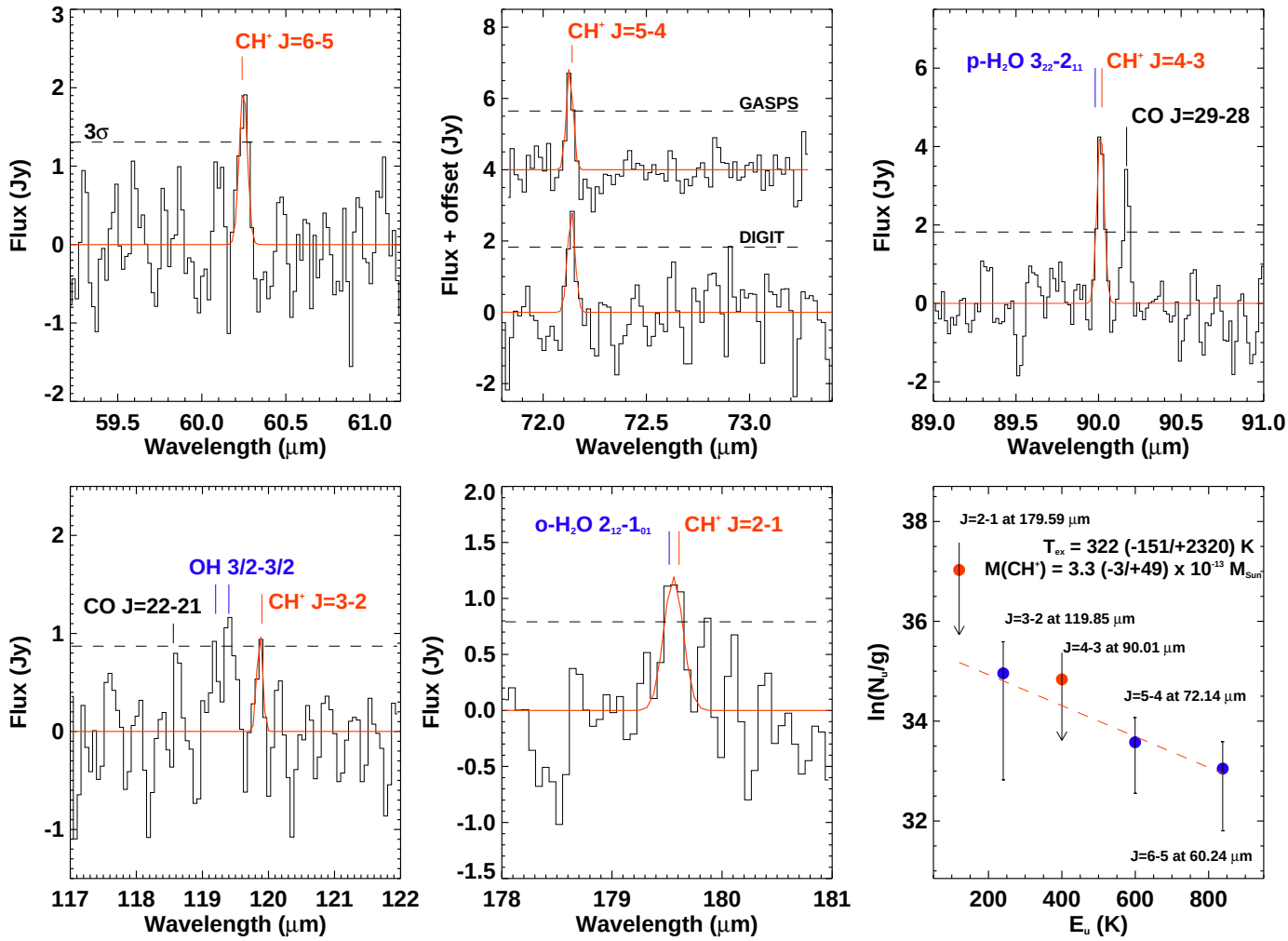

Fig. 1. Continuum-subtracted Herschel-PACS spectra of HD 100546 around the CH^+ J=6–5, 4–3, 3–2, 2–1 (DIGIT data), and J=5-4 (GASPS and DIGIT data) lines. The 3σ statistical error levels do not include the 30% calibration uncertainty. A rotational diagram using those transitions is plotted in the lower-right panel. The errors in the diagram are the quadratic sum of all the statistical and calibration errors ($err_{tot} = \sqrt{(3\sigma_{stat})^2 + (0.3F_{obs})^2}$). Blended lines are considered as upper limits (red filled dots).

ranges (Brittain et al. 2009; Sturm et al. 2010; Panić et al. 2010; Malfait et al. 1998).

2. Herschel observations and rotational diagram

We observed HD 100546 with PACS (Poglitsch et al. 2010) on board the Herschel Space Telescope (Pilbratt et al. 2010) in the 72-73 μm spectroscopic scan range (Δv= 163 km s^{-1}), as part of the open-time key programme GASPS (GaS in Protoplanetary Systems, obsid 1342188437), which aims at a systematic study of gas and dust in discs around stars aged between 0.5 and 30 Myrs. The observations were reduced using the standard pipeline in HIPE 4.2. We detected a line at 72.14 μm that we assign to the rotational J=5-4 emission of CH^+ (see Fig. 1). We also detected the same line in the science demonstration data spectrum taken by the DIGIT team (Sturm et al. 2010), together with the J=6-5 (60.24 μm) and J=3-2 (119.68 μm) lines but with a lower signal-to-noise ratio. It was not possible to strengthen our analysis with detection of either the lowest rotational transition J=1-0, which lies in the SPIRE/HIFI range, or the J=2-1 and J=4-3 lines in the DIGIT dataset, which are blended with water emission lines at the PACS resolution. The ortho H_2O 2_{12}-1_{01} emission at 179.52 μm is blended with the CH^+ J=2-1 line at 179.61 μm, and the para-H_2O 3_{22}-2_{11} at 89.98 μm is blended with the CH^+ J=4-3 line at 90.02 μm. The flux calibration accuracy of the Herschel-PACS instrument is currently 30% in addition to the statistical noise. In addition, flux uncertainties are introduced by difficulties in determining the continuum level in the DIGIT spectra. A new reduction with HIPE 7.0.822, which includes division by the spectral response function and flatfielding, does not improve the noise level in the continuum. The line ratio [O I] 63 μm/CH^+ J=5-4 is 80. We fitted a Gaussian profile to each line. The observed CH^+, [O I], [C II] (Sturm et al. 2010), and CO 3–2 (Panić et al. 2010) fluxes are all reported in Table 1.

We constructed a rotational diagram by assuming LTE population and optically thin emission (see lower right panel of Fig. 1). The level energies, line frequencies, and Einstein spontaneous emission coefficients were computed by Müller (2010) based on the spectroscopic analysis of Amano (2010) . We analysed the diagram using censored data regression and bootstrapping methods. We derived an excitation temperature of 323^{+2320}_{-150} K, a disc-averaged CH^+ column density of $4.3^{+63.8}_{-3.9} \times 10^{12}$ cm^{-2}, consistent with the upper limit found in

Table 1. Observed and modelled line fluxes

Transition	λ (μm)	obs.	model 1 (10^{-17} W m^{-2})	model 2
[O I] $^3P_1$–$^3P_2$	63.19	554.37 ± 167[a]	785	763
[O I] $^3P_0$–$^3P_1$	145.54	35.70 ± 11.4	35.7	42.7
[C II] $^2P_{3/2}$–$^2P_{1/2}$	157.75	31.87 ± 10.0	12.7	17.2
p-H_2O $3_{22}-2_{11}$	89.90	≤ 14.32 ± 5.6[b]	4.6	7.4
CH^+ $J = 4-3$	90.02	≤ 14.32 ± 5.6[b]	3.7	6.3
CH^+ $J = 6-5$	60.25	10.32 ± 5.7	4.2	8.9
CH^+ $J = 5-4$[c]	72.14	6.86 ± 3.4	3.3	6.7
CH^+ $J = 3-2$	119.87	2.16 ± 1.1	1.8	2.9
CO $J = 3-2$[d]	866.96	0.10 ± 0.03	0.08	0.24

[a] The total (3σ statistical + 30% calibration) errors are given for the PACS observations. [b] The blended H_2O+CH^+ line is detected. [c] The PACS values are from the DIGIT programme (Sturm et al. 2010) except for the CH^+ $J = 5-4$ flux (GASPS programme). [d] Data from Panić et al. (2010) with 3σ error.

Table 2. Model parameters.

	MCFOST[a] inner disc	surf. layer	outer disc
Inner radius R_{in} (AU)	0.24	13	13
Outer radius R_{out} (AU)	4	50	500
Surf. density exponent q	1	0.5	1.125
Scale height H_{100AU} (AU)	6	14[a]	14[a]
Scale height exponent β	1.0	1.0	1.0
Total dust mass M_{dust} ($M_\odot$)	1.75(-10)[b]	3(-7)	4.3(-4)
Dust mass ($a \leq$ 1mm, $M_\odot$)	1.75(-10)	3(-7)	1.3(-4)
Min. grain radius a_{min} (μm)	0.1	0.05	1
Max. grain radius a_{max} (μm)	5	1	10^4
Grain power law index p	3.5	3.5	3.5
Silicate grain density (g cm^{-3})	3.0	3.0	3.0
ProDiMo[c]			
ISM UV field (χ, Habing)	1.0		
viscosity (α)	0.0		
Non-thermal speed (km s^{-1})	0.15		
Disc inclination (°)	42		
UV excess	0.013		
UV power-law index	6.5		
Cosmic ray flux ζ(s^{-1})	1(-17)		
PAH $C_{150}H_{30}$ mass ($M_\odot$)	1.8(-7)		
Gas mass ($M_\odot$)	5(-4) (model 1)		
Gas mass ($M_\odot$)	1(-3) (model 2)		

[a] Values taken from Benisty et al. (2010) and Tatulli et al. (2011) except for the scale height H_{100AU} at 100 AU. [b] $\alpha(-\beta)$ means $\alpha \times 10^{-\beta}$. [c] This work.

observing CH^+ at 4232.7 Å (Martin-Zaïdi et al., submitted), and a lower limit to the CH^+ mass of $3.3^{+48.9}_{-3.0} \times 10^{-13}$ $M_\odot$. The CH^+ emitting gas is warm, which suggests that CH^+ is located within 100 AU of the star. The CH^+ abundance is $\geq 3.9 \times 10^{-9}$ relative to an upper limit of warm molecular gas from the VISIR H_2 $S(1)$ 17 μm observation of M(T_{gas}=300 K)$\leq 8.4 \times 10^{-5}$ $M_\odot$ (Martin-Zaïdi et al. 2010).

3. Modelling the physics and chemistry of CH^+

We first fitted the spectral energy distribution (SED) and infrared interferometric VLT-AMBER and MIDI data to constrain the dust properties and the disc structure with a hydrostatic disc using the MCFOST radiative transfer code (Pinte et al. 2006, 2009). The details of the fit are discussed in Benisty et al. (2010) and Tatulli et al. (2011, submitted). The disc is composed of three parts: the inner disc, the outer disc, and an upper layer on the top of the outer disc (see Table 2, Fig. A.1, and the sketch in Benisty et al. 2010). The inner and outer discs are separated by a gap (Bouwman et al. 2003; Grady et al. 2005). The fit to the SED in Tatulli et al. (2011) suggests a scale height value of 10 AU at 100 AU, which is consistent with the scattered-light images, but equally good fits can also be obtained with other values. Therefore we tried several disc structures by varying the scale height H_{100AU}. Using the disc structures derived from the fit to the SED, we modelled the gas chemistry and radiative transfer in the HD 100546 disc with the ProDiMo code (Woitke et al. 2009; Kamp et al. 2010). The ProDiMo code computes the chemistry and heating-cooling balance of the gas self-consistently. We assumed a non-viscous gas (α=0) and a PAH mass ($C_{150}H_{30}$) that is consistent with the strong PAH emissions in the IR (Keller et al. 2008). Large PAHs (≥ 100 carbon atoms) exhibit a strong feature between 10.9 and 11.3 μm (Bauschlicher et al. 2009) as seen in the spectrum of HD 100546. The amount of PAH influences both the thermal state of the disc and the ionisation state of the upper layers. The non-thermal line width is constrained by the resolved CO 3-2 profile. We used a dereddened FUSE and IUE UV spectrum as input to the gas modelling (Martin-Zaïdi et al. 2008). We also ran a ProDiMo model where the disc vertical structure is calculated according to the gas pressure and found that the height of the rim at 13 AU is consistent with the fixed three-part structure.

The main CH^+ formation reaction $C^+ + H_2 \rightarrow CH^+ + H$ (reaction 1) is endothermic by 0.398 eV (4537K). The reaction is efficient only at a few 100 K found in shocked or turbulent regions or when H_2 is vibrationally excited (Hierl et al. 1997; Agúndez et al. 2010). The rate for reaction 1 in Herbst & Knudson (1981) underestimates the experimental data by a factor of 2-3, and the UMIST 2006 rate (Woodall et al. 2007) is a factor 7–8 lower than the experimental values. Initial models with a low rate for reaction 1 underpredict the CH^+ abundance by more than a factor 10. We adopted the value suggested by Hierl et al. (1997): $k_1(T) = (7.4 \pm 0.8) \times 10^{-10} e^{-4537/T}$ cm^3 s^{-1}. We also take the enhanced rate for vibrationally-excited molecular hydrogen into account by assuming that the rate is equal to the Langevin collision value of 1.6×10^{-9} cm^3 s^{-1} (Agúndez et al. 2010). The alternative radiative association reaction $C^+ + H \rightarrow CH^+ + h\nu$ has an extremely low rate of $\sim 10^{-16}$-10^{-17} cm^{-3} s^{-1} (Barinovs & van Hemert 2006). The warm and UV-excited gas at the disc atmosphere around a Herbig AeBe star renders reaction 1 fast. CH^+ reacts with H_2 to form CH_2^+, which in turn reacts with H_2 to form CH_3^+. As both exothermic reactions are fast, an enhanced abundance of CH^+ is accompanied by a high abundance of CH_2^+ and CH_3^+, which have not been detected yet. CH^+ can also dissociatively recombine with an electron into C^+ and H or exchange its charge with PAHs. CH^+ is also destroyed upon absorption of UV photons. The absorption cross-section peaks at ~950 Å. Therefore, the photodissociation around a B9.5V star without strong UV excess due to accretion is not as fast as with an interstellar UV field. The photodissociation and photoionisation rates are computed inside the disc using cross-sections taken from van Dishoeck et al. (2006). The steady-state chemistry includes 188 gas and solid species.

We ran several models with disc gas mass between 10^{-4} and 10^{-2} $M_\odot$ and H_{100AU} between 10 and 20 AU (Fig. A.2). In Table 1 we show the three detected line fluxes for CH^+ out of the 15 rotational transitions in the model, the OI and CII fine-structure lines, and the CO 3–2 transition for our preferred models, which have a disc mass of (0.5–1) $\times 10^{-3}$ $M_\odot$ and

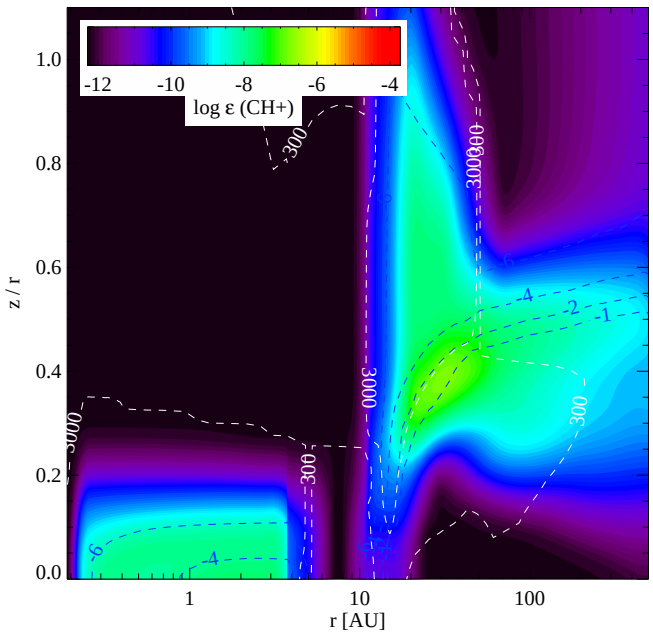

Fig. 2. CH^+ abundance structure in the HD 100546 disc with respect to the number of H-nuclei. The H_2 abundance relative to total H-nuclei abundance contours in log-scale are overplotted in blue, while the T_{gas}=300 and 3000K contours are overplotted in white. The line-of-sight CH^+ observations in the UV would cross the disc at z/r=0.9 (42 °).

H_{100AU} = 14 AU, for the outer disc. All the modelled lines agree within a factor 2 with the observations. In particular, the sum of the p-H_2O $3_{22} - 2_{11}$ and CH^+ $J = 4 - 3$ fluxes is consistent with the observed value. The collision rates of CH^+ with electrons were computed by Lim et al. (1999). In the absence of published collision rates with H_2, we scaled the collision rates with He by 1.39 for $J \leq 6$ transitions (Hammami et al. 2009; Turpin et al. 2010).

4. Discussion

The models suggest that CH^+ is mostly located on the rim (10-13 AU) of the outer disc and at the disc surface (Fig. 2). Although CH^+ is abundant in the tenuous inner disc, its amount is insufficient to contribute to the 72.14 μm emission. CH^+ is located where the gas is mostly heated by collisional de-excitations of nascent and UV-pumped H_2^*. Part of the CH^+ is formed by the reaction with excited H_2^*, but the main fraction comes from the reaction of C^+ with thermal H_2 at $T_{gas} > 400$ K. CH^+ reaches a maximum abundance of $\sim 10^{-7}$ just behind the rim and has a total mass of 10^{-13}-10^{-12} $M_\odot$. The disc average CH^+ abundance is (0.7-7) $\times 10^{-9}$ relative to H-nuclei, consistent with the simple analysis in Sect. 2. The high CH^+ abundance in the rim region and upper disc layers where hydrogen is in atomic form does not affect the C^+ abundance much, which reaches 10^{-4}. However below the disc atmosphere, H_2 self-shielding is efficient, and C^+ is converted rapidly into CH^+. The formation reaction of CH^+ (C^++H_2) competes with the recombination reaction of C^+ to form neutral carbon.

Warm OH (Sturm et al. 2010) and fluorescent ro-vibrational CO emission (Brittain et al. 2009; van der Plas et al. 2009) have also been detected in HD 100546 . OH is mostly formed by the reaction of atomic oxygen O with thermally hot H_2 and vibrationally excited H_2^*. The presence of hot CO, CH^+ and OH supports the idea that hot and excited gas chemical reactions occur on disc surfaces and at the inner rim.

5. Conclusions

We detected the J=5-4 rotational transition of CH^+ at 72.16 μm in two Herschel datasets. We also tentatively detected other lines from CH^+ at 60.25 and 119.87 μm. Other CH^+ lines are blended with water lines. We modelled the CH^+ line fluxes using the most recent chemical and collisional rates. Searches for CH^+ in other Herbig AeBe discs are warranted to test whether the presence of CH^+ is unique to HD 100546 or if it is related to the presence of a high temperature rim of gas, or both.

Acknowledgements. The Grenoble group acknowledges PNPS, CNES, and ANR (contract ANR-07-BLAN-0221). C. Eiroa and G. Meeus are partly supported by the Spanish grant AYA 2008-01727. C. Pinte acknowledges the funding from the EC 7th Framework Programme (PIEF-GA-2008-220891, PERG06-GA-2009-256513). I. Pascucci, M. Grady, S. Brittain, C. Howard, and G. Sandell acknowledge NASA/JPL.

References

Agúndez, M., Goicoechea, J. R., Cernicharo, J., Faure, A., & Roueff, E. 2010, ApJ, 713, 662
Amano, T. 2010, ApJ, 716, L1
Armitage, P. J. 2010, Astrophysics of Planet Formation, ed. Armitage, P. J.
Barinovs, Ğ. & van Hemert, M. C. 2006, ApJ, 636, 923
Bauschlicher, C. W., Peeters, E., & Allamandola, L. J. 2009, ApJ, 697, 311
Benisty, M., Tatulli, E., Ménard, F., & Swain, M. R. 2010, A&A, 511, A75+
Bergin, E. A., Aikawa, Y., Blake, G. A., & van Dishoeck, E. F. 2007, Protostars and Planets V, 751
Bouwman, J., de Koter, A., Dominik, C., & Waters, L. B. F. M. 2003, A&A, 401, 577
Brittain, S. D., Najita, J. R., & Carr, J. S. 2009, ApJ, 702, 85
Carr, J. S. & Najita, J. R. 2008, Science, 319, 1504
Cernicharo, J., Liu, X., Gonzalez-Alfonso, E., et al. 1997, ApJ, 483, L65+
Dutrey, A., Guilloteau, S., & Guelin, M. 1997, A&A, 317, L55
Falgarone, E., Ossenkopf, V., Gerin, M., et al. 2010, A&A, 518, L118+
Falgarone, E., Phillips, T. G., & Pearson, J. C. 2005, ApJ, 634, L149
Gerin, M., de Luca, M., Goicoechea, J. R., et al. 2010, A&A, 521, L16+
Grady, C. A., Woodgate, B., Heap, S. R., et al. 2005, ApJ, 620, 470
Habart, E., Dartois, E., Abergel, A., et al. 2010, A&A, 518, L116+
Hammami, K., Owono Owono, L. C., & Stäuber, P. 2009, A&A, 507, 1083
Henning, T., Semenov, D., Guilloteau, S., et al. 2010, ApJ, 714, 1511
Herbst, E. & Knudson, S. 1981, ApJ, 245, 529
Hierl, P. M., Morris, R. A., & Viggiano, A. A. 1997, J. Chem. Phys., 106, 10145
Kamp, I., Tilling, I., Woitke, P., Thi, W., & Hogerheijde, M. 2010, A&A, 510, A18+
Keller, L. D., Sloan, G. C., Forrest, W. J., et al. 2008, ApJ, 684, 411
Lahuis, F., van Dishoeck, E. F., Boogert, A. C. A., et al. 2006, ApJ, 636, L145
Lim, A. J., Rabadán, I., & Tennyson, J. 1999, MNRAS, 306, 473
Malfait, K., Waelkens, C., Waters, L. B. F. M., et al. 1998, A&A, 332, L25
Martin-Zaïdi, C., Augereau, J., Ménard, F., et al. 2010, A&A, 516, A110+
Martin-Zaïdi, C., Deleuil, M., Le Bourlot, J., et al. 2008, A&A, 484, 225
Müller, H. S. P. 2010, A&A, 514, L6+
Naylor, D. A., Dartois, E., Habart, E., et al. 2010, A&A, 518, L117+
Öberg, K. I., Qi, C., Fogel, J. K. J., et al. 2010, ApJ, 720, 480
Panić, O., van Dishoeck, E. F., Hogerheijde, M. R., et al. 2010, A&A, 519, A110+
Pascucci, I. & Sterzik, M. 2009, ApJ, 702, 724
Pilbratt, G. L., Riedinger, J. R., Passvogel, T., et al. 2010, A&A, 518, L1+
Pinte, C., Harries, T. J., Min, M., et al. 2009, A&A, 498, 967
Pinte, C., Ménard, F., Duchêne, G., & Bastien, P. 2006, A&A, 459, 797
Poglitsch, A., Waelkens, C., Geis, N., et al. 2010, A&A, 518, L2+
Pontoppidan, K. M., Salyk, C., Blake, G. A., et al. 2010, ApJ, 720, 887
Qin, S., Schilke, P., Comito, C., et al. 2010, A&A, 521, L14+
Semenov, D., Pavlyuchenkov, Y., Schreyer, K., et al. 2005, ApJ, 621, 853
Sturm, B., Bouwman, J., Henning, T., et al. 2010, A&A, 518, L129+
Thi, W., van Zadelhoff, G., & van Dishoeck, E. F. 2004, A&A, 425, 955
Turpin, F., Stoecklin, T., & Voronin, A. 2010, A&A, 511, A28+
van den Ancker, M. E., The, P. S., Tjin A Djie, H. R. E., et al. 1997, A&A, 324, L33
van der Plas, G., van den Ancker, M. E., Acke, B., et al. 2009, A&A, 500, 1137

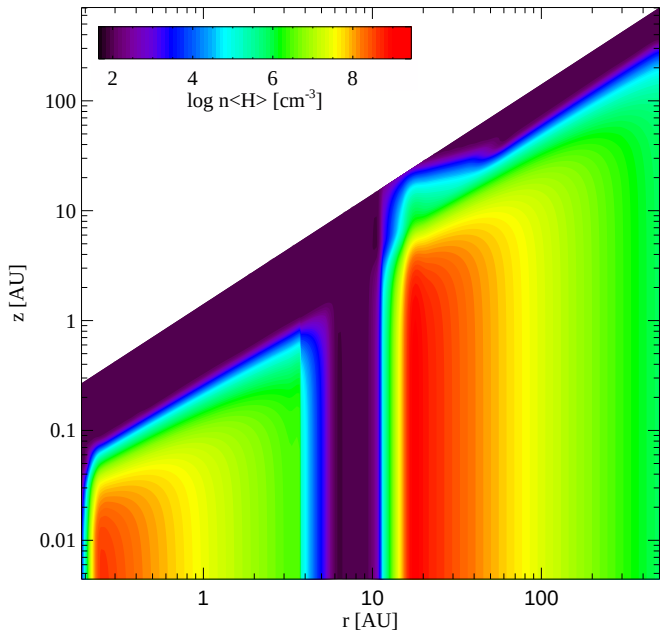

Fig. A.1. The input disc density structure for model 2 constrained by the fit to the SED (see Tatulli et al. 2011 for details). The gap is filled with a gas at density of n_H=100 cm^{-3}.

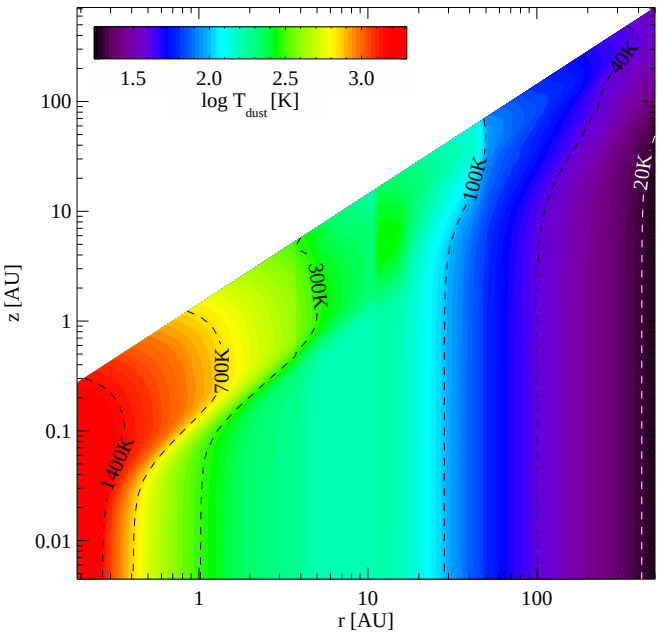

Fig. A.2. The disc dust temperature profile computed by MCFOST for model 2.

van Dishoeck, E. F., Jonkheid, B., & van Hemert, M. C. 2006, Faraday Discussions, 133, 231
van Zadelhoff, G.-J., van Dishoeck, E. F., Thi, W.-F., & Blake, G. A. 2001, A&A, 377, 566
Woitke, P., Kamp, I., & Thi, W. 2009, A&A, 501, 383
Woodall, J., Agúndez, M., Markwick-Kemper, A. J., & Millar, T. J. 2007, A&A, 466, 1197

Appendix A: Disc density and gas temperature structure

We provide for completeness the disc density and the dust and gas temperature structures for model 2 (Fig. A.1, A.2, and A.3).

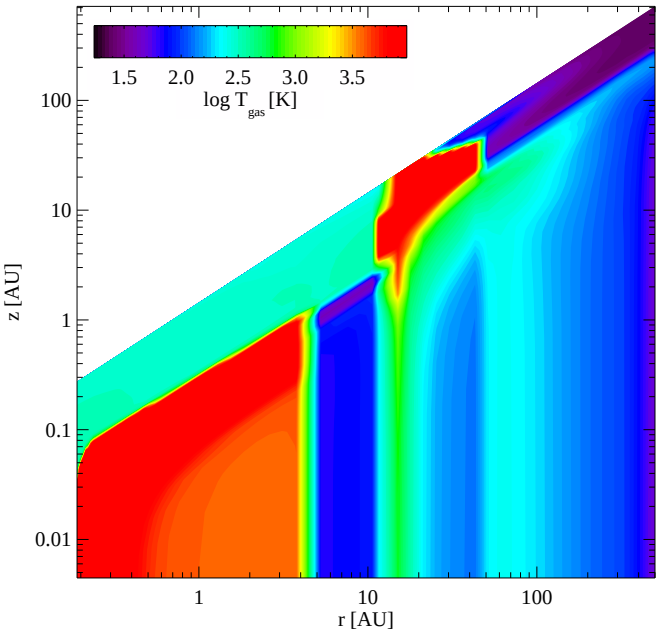

Fig. A.3. The disc gas temperature profile computed by ProDiMo for model 2.